Nanoparticles for Imaging Cartilage

DOI: 10.1002/anie.201404519

Tantalum Oxide Nanoparticles for the Imaging of Articular Cartilage Using X-Ray Computed Tomography: Visualization of Ex Vivo/ In Vivo Murine Tibia and Ex Vivo Human Index Finger Cartilage**

*Jonathan D. Freedman, Hrvoje Lusic, Brian D. Snyder, and Mark W. Grinstaff**

Abstract: *The synthesis and characterization of tantalum oxide (Ta_2O_5) nanoparticles (NPs) as new X-ray contrast media for microcomputed tomography (μCT) imaging of articular cartilage are reported. NPs, approximately 5–10 nm in size, and possessing distinct surface charges, were synthesized using phosphonate (neutral), ammonium (cationic), and carboxylate (anionic) ligands as end functional groups. Assessment of a cartilage defect in a human cadaver distal metacarpophalangeal (MCP) joint with the ammonium nanoparticles showed good visualization of damage and preferential uptake in areas surrounding the defect. Finally, an optimized nontoxic cationic NP contrast agent was evaluated in an in vivo murine model and the cartilage was imaged. These nanoparticles represent a new type of contrast agent for imaging articular cartilage, and the results demonstrate the importance of surface charge in the design of nanoparticulate agents for targeting the surface or interior zones of articular cartilage.*

Nanoparticles (NPs) display distinct properties apart from individual atoms or bulk material as a consequence of their composition, small diameter, high surface area, and confined electronic structure.[1] In medicine, NPs are currently investigated as delivery vehicles for pharmacologically active agents,[2] as reagents for diagnostic assays,[3] as biosensors,[4] and as imaging contrast agents for MRI, fluorescence, PET, and X-ray.[5] For X-ray applications, NPs containing gold, bismuth, and tantalum are used as contrast media for contrast-enhanced computed tomography (CECT) to image lymph nodes[6] and the vascular system.[7] Tantalum is an attractive contrast agent material for CT imaging because it has a higher K-edge (67.4 keV) than conventional iodinated contrast agents (K-edge 33.2 keV) and thus absorbs a greater fraction of the X-rays produced at clinical scanning voltages (80–140 keV). The higher K-edge also decreases low-energy filtration and lessens beam hardening artifacts. In addition, tantalum NPs are biocompatible and have been used successfully in murine in vivo imaging models.[6,7c–e,8] Commonly, tantalum is incorporated in the form of core–shell tantalum oxide (Ta_2O_5) NPs, where the radiopaque Ta_2O_5 core is surrounded by functionalized silane ligands. This class of NPs can be easily modified at the surface and produces stable, low-viscosity nanoparticle suspensions in aqueous physiological conditions. Given our interest in imaging articular cartilage—the smooth, hydrated tissue that lines the ends of bones in load-bearing joints—in order to ascertain the thickness, morphology, and biochemical state, we are designing Ta_2O_5 NPs as contrast agents for imaging cartilage. Herein, we report the synthesis and characterization of phosphonate- (**1**), ammonium- (**2**), and carboxylate(**3**)-functionalized core–shell Ta_2O_5 NPs, the imaging of ex vivo and in vivo murine cartilage, the kinetics of NP penetration into cartilage as a function of surface charge, and the detection of an osteoarthritic defect in a human cadaver metacarpophalangeal (MCP) joint.

Articular cartilage is a three-dimensional collagen (10–20 wt%)[9] matrix that readily absorbs water (68–85 wt%). The hydrated state of articular cartilage is maintained by heavily sulfated and carboxylated glycosaminoglycans (GAGs, 5–10 wt%) that grant cartilage a fixed negative charge. The loss of GAGs in cartilage is a sign of disease,[10] and correlates to worsening mechanical properties[11] and further degradation of the joint soft tissues and bone. Thus, imaging methods using targeted contrast agents that evaluate changes in ex vivo or in vivo cartilage or bone are of interest.[12] For cartilage, measurements of thickness, morphology, and/or GAG content are useful for assessing joint health and diagnosing diseases such as osteoarthritis (OA).[12b–d,13] We hypothesize that ammonium-functionalized, positively charged Ta_2O_5 NPs **2** will accumulate in and provide higher-contrast images of the articular cartilage tissue as a consequence of the fixed-negative charge of the GAGs, compared to the neutral (**1**) or negatively (**3**) charged Ta_2O_5 NPs (see Scheme 1 and Figure SI1).

To investigate the effects of different surface charges, Ta_2O_5 NPs were synthesized possessing different terminal functional groups—phosphonate (neutral; **1**), ammonium (cationic; **2**), and carboxylate (anionic; **3**) (Scheme 1). The synthetic procedure was based on reports by Hyeon et al.[6] and Bonitatibus et al.[7e] (see the Experimental Section for

[*] J. D. Freedman, Dr. H. Lusic, Prof. M. W. Grinstaff
Departments of Biomedical Engineering and Chemistry, and Pharmacology and Experimental Therapeutics
Boston University
Boston, MA 02115 (USA)
E-mail: mgrin@bu.edu
Homepage: http://people.bu.edu/mgrin/
Prof. B. D. Snyder
Center for Advanced Orthopaedic Studies
Beth Israel Deaconess Medical Center, Harvard Medical School
Boston, MA 02115 (USA)

[**] We gratefully acknowledge support in part from the National Institutes of Health (R01GM098361), the T32 Pharmacology Training grant (5T32GM008541-14), and Boston University. We would also like to acknowledge the Center for Advanced Orthopaedic Studies at Beth Israel Deaconess Medical Center for use of their μCT scanner.

Supporting information for this article is available on the WWW under http://dx.doi.org/10.1002/anie.201404519.

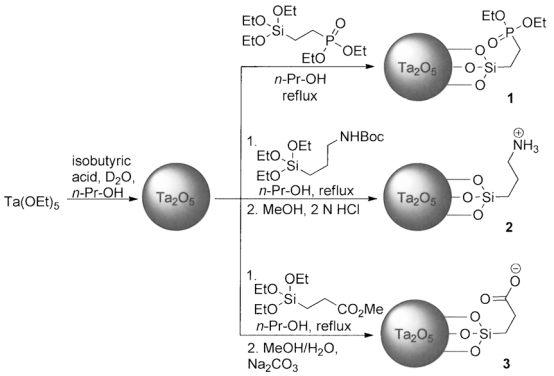

Scheme 1. Synthesis of Ta_2O_5 NPs with neutral phosphonate (NPs **1**), cationic ammonium (NPs **2**), and anionic carboxylate (NPs **3**) ligands at physiological pH.

details). Briefly, the Ta_2O_5 core was formed by hydrolysis of tantalum ethoxide, $Ta(OEt)_5$; the size of the NPs was controlled by the amount of water and isobutyric acid added in *n*-propanol. The silane ligands were subsequently coupled to the NP surface in *n*-propanol under reflux conditions. In the case of NPs **2** and **3**, the final product was obtained after removal of the protecting groups. The ^1H and ^{13}C NMR spectra showed characteristic broad peaks,[7e] which were consistent with the respective ligand for each NP type (Figures SI2–4). The FTIR spectrum of NPs **2** possessed a characteristic ammonium cation absorption band at 2919 cm^{-1} (Figure SI5). Transmission electron microscopy (EM) revealed particles between 5–10 nm in diameter (Figure SI6c). Size determination by scanning EM (Figures 1 and SI6a) was in approximate agreement with dynamic light scattering (DLS) measurements (Table S1, diameter ± standard deviation: NPs **1** = 6.5 ± 0.5 nm, NPs **2** = 3.3 ± 0.7 nm, NPs **3** = 5.0 ± 0.3 nm). Zeta potential measurements revealed distinct charges for each of the NP types (**1**: −1.14 mV, **2**: + 7.58 mV, **3**: −19.07 mV; in pH 7.4).

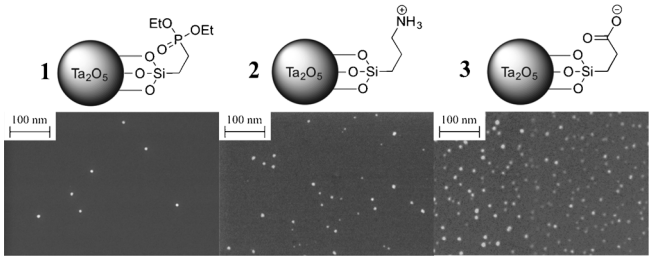

Figure 1. SEM images of Ta_2O_5 NPs with three different silane ligands. Diameter ± standard deviation: NPs **1** = 7.3 ± 2.9 nm, **2** = 6.0 ± 4.4 nm, **3** = 9.6 ± 3.3 nm.

To evaluate the ability of the NPs to serve as contrast media for the imaging of articular cartilage, we serially imaged murine ex vivo proximal tibial cartilage of the knee joint after immersion in a solution of NPs **1**, **2**, and **3**. This cartilage comprises the distal part of the knee joint and is commonly evaluated in murine OA models.[14] Contrast media concentrations of 40 mg NP/mL were chosen based on a pilot imaging experiment showing sufficient attenuation for cartilage imaging and based on the desired signal strength of known small-molecule iodinated CT contrast agents (Figure SI7).[12b] The osmolality of the solutions was balanced to 400 mOsm to match the ionic strength of synovial fluid.[15] As shown in Figure 2, the uptake of NPs **2** was faster and

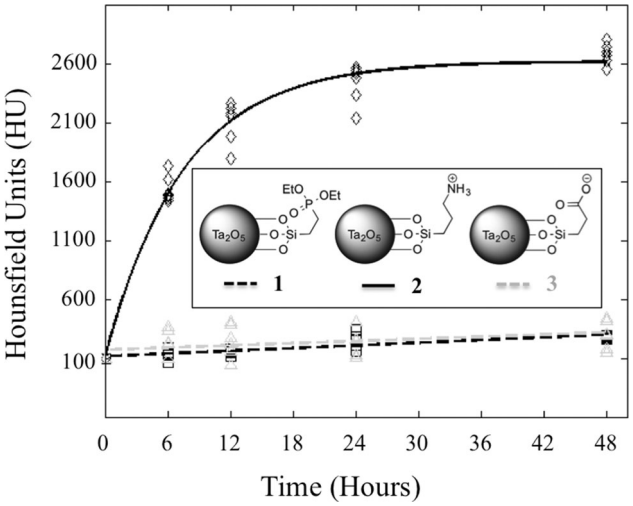

Figure 2. Diffusion of NP contrast agents into mouse tibia over 48 h. Solid lines represent fitted data. NPs **2** (solid black line) produce greater attenuation than NPs **1** (dashed black line) or **3** (dashed gray line) and diffuse into the cartilage in approximately 24 h (> 95% of equilibrium).

significantly greater than that of NPs **1** ($p < 0.0001$), or **3** ($p < 0.0001$), as measured after incubation for 48 h. An exponential function was used to fit the data obtained with NPs **2** [$f(t) = \alpha(1-e^{-t/\tau})$; $\tau = 7.5$ h] showing that diffusion leveled out (> 95% of equilibrium) after 24 h. NPs **1** and **3** showed slow linear diffusion trends into the cartilage tissue and produced a change of less than 200 HU over 48 h of immersion. The results from the quantitative uptake studies can be visualized, as uptake of NPs **2** provides good visualization of the tibial cartilage in agreement with areas of histological images stained with safranin-O, a standard stain used to mark GAGs in cartilage tissue (Figure SI9b). NPs **2** distributed into the entirety of the articular cartilage, increasing the attenuation and enabling clear visual delineation of cartilage from both air and bone. In addition, NPs **2** also diffused into soft tissue remnants near the tendon insertion sites and were visualized by CECT. NPs **1** and **3** were seen to accumulate at the surface, were largely excluded from the cartilage, and did not produce definitive cartilage–air or cartilage–bone interfaces (Figure 3).

Next, CECT with NPs **2** was used to image a naturally occurring cadaveric osteoarthritic defect in the proximal MCP joint of a human index finger of a 73-year old male. This type of defect is commonly related to overuse, such as typing or texting, and is also associated with advanced age and injury.[16] The joint was baseline imaged and then immersed in 40 mg NP/mL of NPs **2** for 24 h and then re-imaged. In baseline 3D and 2D CT images, the overall attenuation of

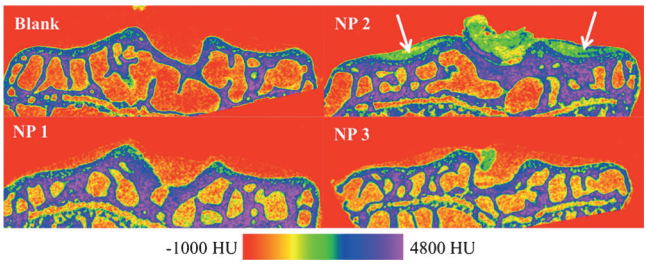

Figure 3. 2D coronal CT cross-sections of mouse tibia plateau articular cartilage after 48 hours of exposure to NP contrast agents compared to a nonexposed (blank) specimen (6 μm resolution). NPs **2** show a clear visualization of cartilage on the lateral and medial tibial plateaus (white arrows) as well as some midline remnant soft tissue ligaments that have also been shown to possess GAG content. NPs **1** and **3** uptake into the articular cartilage is poor and it is difficult to differentiate between air and cartilage in the image reconstructions.

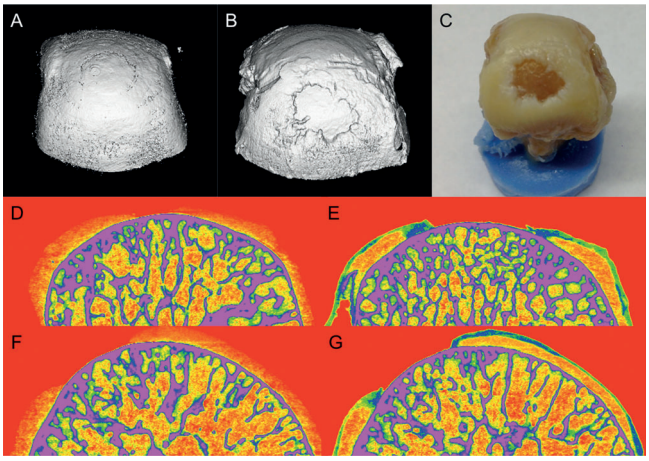

Figure 4. Cartilage defect in the proximal metacarpophalangeal (MCP) joint of a human index finger is clearly visualized only in the presence of NPs **2**. The MCP was imaged before (A,D,F) and after (B,E,G) immersion in 40 mg NP/mL of NPs **2** for 24 h. The 3D CT reconstruction (B) shows the defect and is similar to that seen with gross inspection (C). Coronal (D and E) and sagittal (F and G) cross-section 2D-CT reconstructions are also shown, which further document the requirement of using NPs **2** to visualize the cartilage and the defect in the MCP.

cartilage is low and the boundaries between bone, cartilage, and air are poorly resolved (Figure 4: A, D, F). On the other hand, the contrast-enhanced images exhibited high attenuation and showed penetration of NPs **2** into in the areas of roughened cartilage and the defect could be clearly visualized (Figure 4: B, E, G). In the sample imaged, the large defect closely matched the area of exposed bone and irregular cartilage edges as seen on gross inspection after disarticulation (Figure 4C).

In areas of the MCP joint where the cartilage tissue was intact, NPs **2** accumulated throughout the tissue but were concentrated at the surface of the cartilage. The penetration of NPs **2** into human cartilage appears to be different than that in mouse cartilage, and this may be a consequence of the different cartilage pore sizes or compositional differences. Nonetheless, contrast agents that analyze the surface morphology of articular cartilage and surrounding soft tissue are useful to detect defects such as cartilage lesions[13b] and labrum tears.[17]

NPs **2** possess a positive charge and in general, positively charged NPs are more cytotoxic than neutral materials.[18] Our preliminary assessment agrees with this as NPs **2** and **3** exhibited moderate cytotoxicity (80–60%) against 3T3 fibroblasts after 4 h (Figure SI 11) and the results were comparable to those obtained with ioxaglate, an FDA-approved and clinically used iodinated CT agent (Figure SI 12). Given this result, we further optimized the NP surface coating to contain (short) poly(ethylene glycol) (PEG) ligands and a tetraammonium group (1:1), where the ammonium group ensures a cationic charge and the PEG reduces the cytotoxicity (NPs **4**; Figure 5). NPs **4** exhibit an improved cytotoxicity profile

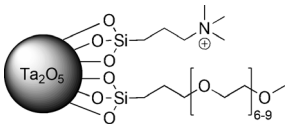

Figure 5. Tantalum oxide NPs with tetraammonium and (short) PEG ligands (NP **4**).

compared to NPs **2**, and are non-cytotoxic, being similar to the untreated control (Figure SI 13). NPs **4** allow the visualization of ex vivo cartilage similar to NPs **2** (Figure SI 13b). Intravenous injection of NPs **4** (1 mL of 40 mg mL^{-1}) showed high contrast in the calyces of the kidneys after 15 min, which suggests that renal clearance and no accumulation in the liver or spleen occurs. This result is consistent with those for other nanoparticles of this size.[19] The delivery route was chosen over intra-articular injection to ensure sufficient material for CT imaging.

To demonstrate the in vivo feasibility, NPs **4** were injected intra-articularly into the knee of an adult male Wistar rat (100 μL of 40 mg mL^{-1}). This delivery approach ensures a high concentration of contrast agent in the local cartilage area and minimizes systemic exposure. At the same time less injected material is required compared to an intravenous (IV) injection to obtain the same contrast agent concentration in the joint. This procedure (arthrography) is currently performed clinically with iodinated CT contrast agents for imaging of the cartilage. The knee was flexed five times to facilitate diffusion of the contrast agent throughout the joint and scanned by low-resolution peripheral quantitative computed tomography (pQCT) (100 μm^2 in plane). In a composite colorized axial CT image, showing the bone in grayscale, the contrast can be seen in green throughout the joint space and is concentrated at specific cartilage regions at the bone interface (Figure 6A). A similar in vivo result was observed with the other cationic NPs **2** (Figure SI 14). After in vivo imaging, the rat was allowed to recover and displayed no signs of distress. The rat was then immediately sacrificed and the joint scanned by high-resolution μCT (36 μm^3 isotropic). Similarly, the equivalent ex vivo axial image shows contrast throughout the joint as well as throughout the cartilage and penetrating it

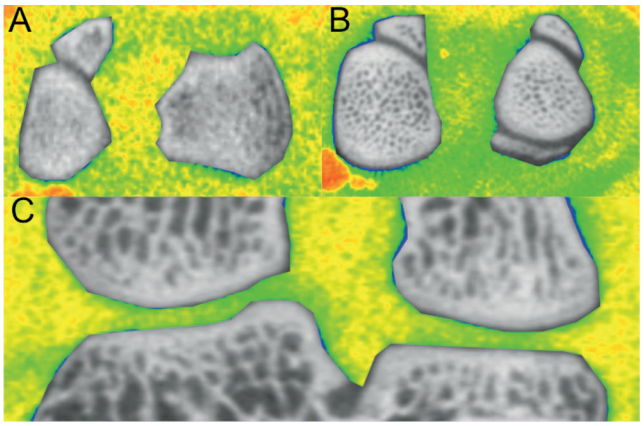

Figure 6. A composite in vivo (A) and ex vivo image (B,C) showing the joint space in color and the bone in grayscale. The contrast (green) can be seen throughout the joint compared to the soft tissue, highlighting the cartilage (A, B) or cartilage, tendon, and meniscus (C). The original, grayscale images can be found in the Supporting Information.

(Figure 6B). The cartilage can be more easily observed in the coronal view shown in Figure 6C, where the cartilage (green) is located between the bone and synovial space. Subsequent histological examination of the cartilage revealed no adverse effects and the results were similar to those of untreated control cartilage.

Ta_2O_5 NPs with significant differences in overall surface charges were synthesized and evaluated as CT contrast media for imaging of murine and human articular cartilage. The positively charged NPs exhibited substantially greater affinity for articular cartilage, due to the favorable coulombic attraction[12b,20] to the fixed, negatively charged GAGs of the cartilage. Moreover, when the positive charge on the NP surface was maintained and a PEG coating was introduced, we obtained a NP formulation **4**, which was successfully used for in vivo cartilage imaging. These results demonstrate the importance of electrostatic-based targeting and transport for nanosized materials into articular cartilage, and show the successful ex vivo and in vivo μCT imaging of articular cartilage with nanoparticulate cationic contrast agents. Furthermore, these findings support the use and further development of μCT imaging (instruments, contrast agents, software) for small-animal models to provide both quantitative and 3D spatial assessment of cartilage, which is conventionally assessed qualitatively with 2D histology and precluded from MR imaging due to resolution limitations. Such tools are immediately of interest for the preclinical evaluation of pharmacological agents, biologics, and tissue engineering strategies for the treatment of osteoarthritis and for the future development of CT agents to assist in the diagnosis of osteoarthritis in the clinic.

Experimental Section

Ethyl phosphonate tantalum oxide NPs (**1**). The NPs were synthesized according to the literature procedure.[7e] ^{1}H NMR (400 MHz, D_2O): $\delta = 0.69$ (br s, 2H), 1.19 (br s, 3H), 1.72 (br s, 2H), 4.00 ppm (br s, 2H). ^{31}P NMR (162 MHz, D_2O): $\delta = 36.3$ ppm (br s). FTIR: $\tilde{\nu}$ =1444 (weak), 1412 (weak), 1273 (weak), 1215 (strong), 1165 (medium), 1094 (weak), 1020 (very strong), 938 (very strong), 777 cm^{-1} (strong). ICP-AES: Ta/Si (wt/wt) 2.08 ± 0.02.

(*n*-Propylamine HCl salt) tantalum oxide NPs (**2**). Isobutyric acid (0.44 mL) and D_2O (0.5 mL) were added to *n*-propanol (34 mL). Tantalum(V) ethoxide (1.87 g, 1.19 mL) was added dropwise at a rate of 0.2 mL min^{-1}, and the solution was left to stir for 16 h at RT under an N_2 atmosphere. The solution was then diluted by addition of *n*-propanol (20 mL), followed by addition of *tert*-butyl 3-(triethoxysilyl)propylcarbamate (5 g) in *n*-propanol (15 mL) at a rate of 1 mL min^{-1}. The reaction was subsequently heated at reflux for 2 h and then cooled to RT. Next, NH_4OH (0.1 M, 250 mL) was added to the solution, and the reaction mixture was stirred for 16 h at RT. Subsequently, H_2O (40 mL) and aq. HCl (1.2 M, 10 mL) were added to the flask dropwise over 20 min. The reaction was then allowed to proceed at 50 °C for 48 h. The mixture was cooled to RT and filtered through a 0.22 μm membrane, and the volatiles were evaporated. The residue was redissolved in MeOH (50 mL) and cooled to 0 °C. A solution of 2 N HCl (50 mL) was added to the flask and the reaction was stirred at RT for 48 h. The solution was neutralized to pH 7 by addition of Na_2CO_3, filtered through a 0.22 μm membrane, and then transferred into dialysis tubing (MWCO 3.5 kDa). The product was purified by dialysis for 72 h with frequent water changes. The removal of volatiles by lyophilization afforded **2** as a white powder. ^{1}H NMR (400 MHz, D_2O): $\delta = 0.53$ (br s, 2H), 1.64 (br s, 2H), 2.89 ppm (br s, 2H). ^{13}C NMR (100 Hz, D_2O): $\delta = 9.7, 21.0, 41.7$ ppm. FTIR: $\tilde{\nu}$ =3320 (weak), 2919 (very strong), 1611 (medium), 1502 (medium), 1210 (weak), 1044 (weak), 922 (strong), 802 cm^{-1} (weak). ICP-AES: Ta/Si (wt/wt) 4.96 ± 0.06.

Sodium propanoate tantalum oxide NPs (**3**). Isobutyric acid (0.44 mL) and D_2O (0.5 mL) were added to *n*-propanol (34 mL). Tantalum(V) ethoxide (1.87 g, 1.19 mL) was added dropwise at a rate of 0.2 mL min^{-1}, and the solution was left to stir for 16 h at RT, under N_2 atmosphere. The mixture was diluted by addition of *n*-propanol (20 mL), followed by addition of methyl 3-(triethoxysilyl)propanoate (5 g) in *n*-propanol (15 mL) at a rate of 1 mL min^{-1}. The reaction mixture was kept at reflux for 2 h, then cooled to RT, and NH_4OH (0.1 M, 250 mL) was added. After stirring at RT for 16 h, H_2O (40 mL) and aq. HCl (1.2 M, 10 mL) were added to the flask dropwise over 20 min. The reaction was then allowed to proceed at 50 °C for 48 h. It was cooled to RT and filtered through a 0.22 μm membrane, and the volatiles were evaporated. The residue was redissolved in MeOH (50 mL) and cooled to 0 °C. Deionized water (50 mL) was added, Na_2CO_3 was added to adjust to pH 10, and the reaction mixture was stirred at 40 °C for 48 h. The solution was neutralized by addition of 1 N HCl, filtered through a 0.22 μm membrane, and then transferred into dialysis tubing (MWCO 3.5 kDa). The product was purified by dialysis for 72 h with frequent water changes. The removal of volatiles by lyophilization afforded **3** as a white powder. ^{1}H NMR (400 MHz, D_2O): $\delta = 0.59$ (br s, 2H), 2.00 ppm (br s, 2H). ^{13}C NMR (100 Hz, D_2O): $\delta = 9.2, 30.6, 185.8$ ppm. FTIR: $\tilde{\nu}$ =3265 (weak), 2927 (weak), 1656 (weak), 1562 (strong), 1410 (strong), 1304 (weak), 1187 (weak), 1033 (medium), 912 cm^{-1} (very strong). ICP-AES: Ta/Si (wt/wt) 2.64 ± 0.05.

Tetraammonium-PEG tantalum oxide NPs (**4**). Isobutyric acid (0.44 mL) and D_2O (0.5 mL) were added to *n*-propanol (34 mL). Tantalum(V) ethoxide (1.87 g, 1.19 mL) was added dropwise at a rate of 0.2 mL min^{-1} and the solution was left to stir at RT for 16 h under an N_2 atmosphere. The solution was then diluted with *n*-propanol (20 mL), followed by addition of a mixture of *N*-trimethoxysilylpropyl-*N*,*N*,*N*-trimethylammonium chloride (2.5 g) and 2-[methoxy(polyethylenoxy)propyl]trimethoxysilane (2.5 g) in *n*-propanol (15 mL) at a rate of 1 mL min^{-1}. The reaction mixture was kept at reflux for 2 h and then cooled to RT. NH_4OH (0.1 M, 250 mL) was added, and the mixture was stirred at RT for 16 h. Subsequently, H_2O (40 mL) and aq. HCl (1.2 M, 10 mL) were added dropwise over

20 min. The reaction was then allowed to proceed at 50 °C for 48 h. The solution was neutralized by addition of Na_2CO_3, filtered through a 0.22 μm membrane, and then transferred into dialysis tubing (MWCO 3.5 kDa). The product was purified by dialysis for 72 h with frequent water changes. The removal of volatiles by lyophilization afforded **4** as a white powder. ^{1}H NMR (400 MHz, D_2O): $\delta = 0.10$ (br s), 1.15 (br s), 1.37 (br s), 2.5–3.3 ppm (br m). FTIR: $\tilde{\nu}$ =2871 (strong), 1647 (medium), 1479 cm^{-1} (medium). ICP-AES: Ta/Si (wt/wt) 5.18 ± 0.04.

Received: April 21, 2014
Published online: June 30, 2014

Keywords: cartilage · imaging · nanoparticles · X-ray contrast media

[1] E. Roduner, *Chem. Soc. Rev.* **2006**, *35*, 583 – 592.
[2] P. Wanakule, K. Roy, *Curr. Drug Metab.* **2012**, *13*, 42 – 49.
[3] M. Larguinho, P. V. Baptista, *J. Proteomics* **2012**, *75*, 2811 – 2823.
[4] R. C. Somers, M. G. Bawendi, D. G. Nocera, *Chem. Soc. Rev.* **2007**, *36*, 579 – 591.
[5] a) J. L. Vivero-Escoto, R. C. Huxford-Phillips, W. Lin, *Chem. Soc. Rev.* **2012**, *41*, 2673 – 2685; b) N. Lee, S. H. Choi, T. Hyeon, *Adv. Mater.* **2013**, *25*, 2641 – 2660; c) M. Shilo, T. Reuveni, M. Motiei, R. Popovtzer, *Nanomedicine* **2012**, *7*, 257 – 269; d) H. Lusic, M. W. Grinstaff, *Chem. Rev.* **2013**, *113*, 1641 – 1666; e) N. Lee, T. Hyeon, *Chem. Soc. Rev.* **2012**, *41*, 2575 – 2589; f) A. Louie, *Chem. Rev.* **2010**, *110*, 3146 – 3195; g) E. C. Dreaden, A. M. Alkilany, X. Huang, C. J. Murphy, M. A. El-Sayed, *Chem. Soc. Rev.* **2012**, *41*, 2740 – 2779.
[6] M. H. Oh, N. Lee, H. Kim, S. P. Park, Y. Piao, J. Lee, S. W. Jun, W. K. Moon, S. H. Choi, T. Hyeon, *J. Am. Chem. Soc.* **2011**, *133*, 5508 – 5515.
[7] a) J. T. Au, G. Craig, V. Longo, P. Zanzonico, M. Mason, Y. Fong, P. J. Allen, *AJR Am. J. Roentgenol.* **2013**, *200*, 1347 – 1351; b) O. Rabin, J. Manuel Perez, J. Grimm, G. Wojtkiewicz, R. Weissleder, *Nat. Mater.* **2006**, *5*, 118 – 122; c) A. S. Torres, P. J. Bonitatibus, Jr., R. E. Colborn, G. D. Goddard, P. F. FitzGerald, B. D. Lee, M. E. Marino, *Invest. Radiol.* **2012**, *47*, 578 – 587; d) P. J. Bonitatibus, Jr., A. S. Torres, B. Kandapallil, B. D. Lee, G. D. Goddard, R. E. Colborn, M. E. Marino, *ACS Nano* **2012**, *6*, 6650 – 6658; e) P. J. Bonitatibus, Jr., A. S. Torres, G. D. Goddard, P. F. FitzGerald, A. M. Kulkarni, *Chem. Commun.* **2010**, *46*, 8956 – 8958; f) Q. Xiao, W. Bu, Q. Ren, S. Zhang, H. Xing, F. Chen, M. Li, X. Zheng, Y. Hua, L. Zhou, W. Peng, H. Qu, Z. Wang, K. Zhao, J. Shi, *Biomaterials* **2012**, *33*, 7530 – 7539.
[8] N. Lee, H. R. Cho, M. H. Oh, S. H. Lee, K. Kim, B. H. Kim, K. Shin, T. Y. Ahn, J. W. Choi, Y. W. Kim, S. H. Choi, T. Hyeon, *J. Am. Chem. Soc.* **2012**, *134*, 10309 – 10312.
[9] V. C. Mow, R. Huiskes, *Basic Orthopaedic Biomechanics and Mechano-Biology*, 3edrd edLippincott Williams & Wilkins, Philadelphia, **2005**.
[10] D. T. Felson, R. C. Lawrence, P. A. Dieppe, R. Hirsch, C. G. Helmick, J. M. Jordan, R. S. Kington, N. E. Lane, M. C. Nevitt, Y. Zhang, M. Sowers, T. McAlindon, T. D. Spector, A. R. Poole, S. Z. Yanovski, G. Ateshian, L. Sharma, J. A. Buckwalter, K. D. Brandt, J. F. Fries, *Ann. Intern. Med.* **2000**, *133*, 635 – 646.
[11] B. A. Lakin, D. J. Grasso, S. S. Shah, R. C. Stewart, P. N. Bansal, J. D. Freedman, M. W. Grinstaff, B. D. Snyder, *Osteoarthr. Cartilage* **2013**, *21*, 60 – 68.
[12] a) R. Parkesh, W. Gowin, T. C. Lee, T. Gunnlaugsson, *Org. Biomol. Chem.* **2006**, *4*, 3611 – 3617; b) N. S. Joshi, P. N. Bansal, R. C. Stewart, B. D. Snyder, M. W. Grinstaff, *J. Am. Chem. Soc.* **2009**, *131*, 13234 – 13235; c) T. S. Silvast, H. T. Kokkonen, J. S. Jurvelin, T. M. Quinn, M. T. Nieminen, J. Toyras, *Phys. Med. Biol.* **2009**, *54*, 6823 – 6836; d) A. W. Palmer, R. E. Guldberg, M. E. Levenston, *Proc. Natl. Acad. Sci. USA* **2006**, *103*, 19255 – 19260; e) M. Yin, J. Shen, G. O. Pflugfelder, K. Mullen, *J. Am. Chem. Soc.* **2008**, *130*, 7806 – 7807; f) C. S. Winalski, S. Shortkroff, E. Schneider, H. Yoshioka, R. V. Mulkern, G. M. Rosen, *Osteoarthr. Cartilage* **2008**, *16*, 815 – 822.
[13] a) H. T. Kokkonen, J. S. Jurvelin, V. Tiitu, J. Toyras, *Osteoarthr. Cartilage* **2011**, *19*, 295 – 301; b) J. Hirvasniemi, K. A. Kulmala, E. Lammentausta, R. Ojala, P. Lehenkari, A. Kamel, J. S. Jurvelin, J. Toyras, M. T. Nieminen, S. Saarakkala, *Osteoarthr. Cartilage* **2013**, *21*, 434 – 442; c) J. van Tiel, M. Siebelt, J. H. Waarsing, T. M. Piscaer, M. van Straten, R. Booij, M. L. Dijkshoorn, G. J. Kleinrensink, J. A. Verhaar, G. P. Krestin, H. Weinans, E. H. Oei, *Osteoarthr. Cartilage* **2012**, *20*, 678 – 685; d) K. A. Kulmala, R. K. Korhonen, P. Julkunen, J. S. Jurvelin, T. M. Quinn, H. Kroger, J. Toyras, *Med. Eng. Phys.* **2010**, *32*, 878 – 882; e) H. J. Yoo, S. H. Hong, J. Y. Choi, I. J. Lee, S. J. Kim, J. A. Choi, H. S. Kang, *Radiology* **2011**, *261*, 805 – 812; f) P. N. Bansal, N. S. Joshi, V. Entezari, M. W. Grinstaff, B. D. Snyder, *Osteoarthr. Cartilage* **2010**, *18*, 184 – 191; g) P. N. Bansal, N. S. Joshi, V. Entezari, B. C. Malone, R. C. Stewart, B. D. Snyder, M. W. Grinstaff, *J. Orthop. Res.* **2011**, *29*, 704 – 709; h) P. N. Bansal, R. C. Stewart, V. Entezari, B. D. Snyder, M. W. Grinstaff, *Osteoarthr. Cartilage* **2011**, *19*, 970 – 976; i) L. N. Hayward, C. M. de Bakker, L. C. Gerstenfeld, M. W. Grinstaff, E. F. Morgan, *J. Orthop. Res.* **2013**, *31*, 567 – 573; j) R. C. Stewart, P. N. Bansal, V. Entezari, H. Lusic, R. M. Nazarian, B. D. Snyder, M. W. Grinstaff, *Radiology* **2013**, *266*, 141 – 150.
[14] a) N. Kotwal, J. Li, J. Sandy, A. Plaas, D. R. Sumner, *Osteoarthr. Cartilage* **2012**, *20*, 887 – 895; b) S. M. Botter, G. J. van Osch, S. Clockaerts, J. H. Waarsing, H. Weinans, J. P. van Leeuwen, *Arthritis Rheum.* **2011**, *63*, 2690 – 2699; c) A. S. K. de Hooge, F. A. J. van de Loo, M. B. Bennink, O. J. Arntz, P. de Hooge, W. B. van den Berg, *Osteoarthr. Cartilage* **2005**, *13*, 66 – 73.
[15] M. Baumgarten, R. D. Bloebaum, S. D. K. Ross, P. Campbell, A. Sarmiento, *J. Bone Jt. Surg. Am. Vol.* **1985**, *67A*, 1336 – 1339.
[16] F. M. K. Williams, T. D. Spector, *Medicine* **2006**, *34*, 364 – 368.
[17] Y. Yamamoto, H. Tonotsuka, T. Ueda, Y. Hamada, *Arthroscopy* **2007**, *23*, 1290 – 1294.
[18] a) S. Bhattacharjee, I. M. Rietjens, M. P. Singh, T. M. Atkins, T. K. Purkait, Z. Xu, S. Regli, A. Shukaliak, R. J. Clark, B. S. Mitchell, G. M. Alink, A. T. Marcelis, M. J. Fink, J. G. Veinot, S. M. Kauzlarich, H. Zuilhof, *Nanoscale* **2013**, *7*, 4870 – 4883; b) S. J. Soenen, M. De Cuyper, *Contrast Media Mol. Imaging* **2009**, *4*, 207 – 219.
[19] M. Longmire, P. L. Choyke, H. Kobayashi, *Nanomedicine* **2008**, *3*, 703 – 717.
[20] a) S. Byun, M. D. Tortorella, A. M. Malfait, K. Fok, E. H. Frank, A. J. Grodzinsky, *Arch. Biochem. Biophys.* **2010**, *499*, 32 – 39; b) A. G. Bajpayee, C. R. Wong, M. G. Bawendi, E. H. Frank, A. J. Grodzinsky, *Biomaterials* **2014**, *35*, 538 – 549.

